Cavitation-induced streaming in shock wave lithotripsy

Yuri A. Pishchalnikov[*], **James A. McAteer**

Department of Anatomy and Cell Biology, Indiana University School of Medicine, 635 Barnhill Drive, Indianapolis, IN 46202

Abstract

Cavitation generated by lithotripter shock waves (SWs) in non-degassed water was studied using a 60 frames-per-second camcorder—recording the migration of microbubbles over successive SWs. Lithotripter SWs were produced using a Dornier DoLi-50 electromagnetic lithotripter at 0.5 and 2 Hz pulse repetition frequency (PRF). Cavitation was affected by PRF and by the power level (PL) of the lithotripter. At slow PRF, such as shots fired many seconds apart, cavitation was relatively sparse and bubble clouds flowed in the direction of SW propagation. When PRF was increased, the bubble clouds generated by one SW were amplified by subsequent SWs. Cloud amplification was accompanied by an apparent change in the pattern of bubble migration. Whereas bubbles continued to enter the field of view from the prefocal side, the main bubble cloud remained near the focal point. This was due to a streaming of bubbles opposite to the direction of SW propagation. Increasing the PL grew the cavitation field and enhanced the flow of bubbles opposite to the direction of SW propagation. Stepping up the PL acted to push the broad cloud progressively prefocally (toward the SW source), shifting the position of the plane at which the opposing directional bubble flows collided. (NIH DK43881)

INTRODUCTION

In shock wave lithotripsy (SWL) to break kidney stones shock pulses are typically delivered at rates from 0.5 to 2 Hz pulse repetition frequency (PRF).[1] Higher rates (2Hz PRF) have been observed to generate cavitation clouds with increased number of bubbles.[1–5] This increase is likely because of daughter microbubbles that are produced upon collapse and rebound of cavitation bubbles.[4–5] These daughter microbubbles were seen to migrate across the field, seeding the proliferation of cavitation upon being hit by successive shock waves (SWs).[5] In this work, the migration of microbubbles is investigated in more detail. It is observed that the pattern of bubble migration depended on PRF and power level of the lithotripter. The observations show that cavitation can induce streaming and the induced streaming can be directed opposite to the propagation of lithotripter SWs.

MATERIALS AND METHODS

This study was conducted using a Dornier DoLi-50 electromagnetic lithotripter (Dornier MedTech Systems, Germany). The lithotripter has six power levels (PL1–6) and can deliver

yurapish@gmail.com.

[*]Present address: Impulse Devices, Inc., 13366H Grass Valley Ave., Grass Valley, CA 95945

SWs at up to 2 Hz PRF. The therapy head of the lithotripter was coupled with LithoClear gel (Sonotech, Bellingham, MA, USA) to an acoustically transparent Mylar membrane of a test tank (Figure 1).[6]

The tank was filled with approximately 15 liters of tap water 24 hours prior to the experiments. The dissolved gas and temperature of water were measured using an YSI DO200 oxygen meter (YSI, Inc., Yellow Springs, OH). During the experiments, the water temperature increased slowly from 22 to 24.2 °C. The dissolved oxygen remained at about 98–100% of saturation, and was 8.5 ppm at 22°C and 8.3 ppm at 24.2°C.

Cavitation was recorded using a conventional camcorder (~60 frames per second, 1920×1080 pixels, HDR-HC3, Sony Corp.) as previously described.[5] The video field was calibrated by positioning a ruler along the acoustic axis of the lithotripter. The field of view was approximately 61 mm by 35 mm (Figure 1), providing a spatial resolution of about 32 μm per pixel. The exposure time of the camcorder (~17 ms) was much longer than the growth-collapse cycle of cavitation bubbles (less than 1 ms),[1–5] so that single frames captured cavitation bubbles at all stages throughout the entire growth-collapse cycle. Therefore, frames recorded during the passage of lithotripter SWs show bubbles at their maximum expansion.[5] Other frames, recorded between lithotripter SWs, show minute microbubbles—the size of which (< 10 μm) was difficult to determine even with 2–4 μm/pixel resolutions of a high-speed camera.[4,5]

Minute microbubbles were visualized by minimizing background illumination and maximizing the light scattered from the bubbles. Two twin fiber-optic light sources (KL 1500 LCD, Schott Leica) were positioned above the target zone and oriented perpendicular to the SW axis (Figure 1). This illumination visualized minute microbubbles as bright diffraction spots with the apparent size much larger than the actual microbubbles. The position of these bright spots was recorded by the camcorder and was used to track the motion of the host fluid.

Fluid motion was assessed by tracking small ensembles of neighboring microbubbles—bubble patterns. Bubble pattern displacements were measured by a program written in LabVIEW (National Instruments, Austin, TX). We implemented a Minimum Quadratic Difference algorithm.[7] Bubble patterns were tracked from frame to frame within multiple small sampling areas selected to blanket the field of view. Location of the minimum quadratic difference in pixel brightness was used to find the best match of bubble pattern between frames. Bubble-pattern displacement was divided by the time interval between the frames (0.017 s) to determine flow velocity.

Flow velocities shown in Figures 5–6 were found using the following procedure. First, the original 1920×1080-pixel frames were re-sampled to 1248×702-pixel images giving resolution ≈50 μm/px. Frames from recordings collected at two power levels of the lithotripter (PL2 and PL6) were then combined into single two-panel plates. Sampling areas for the Minimum Quadratic Difference algorithm were 32×16 pixels with the centers of the sampling areas separated 16 pixels apart. To reduce the errors associated with spurious

vectors, the found velocity vector field was averaged using a median procedure such that each 3×3 vector matrix was replaced by a median flow velocity vector.

Lithotripter SWs were measured using a fiber-optic probe hydrophone (FOPH-500, RP Acoustics, Germany). To minimize cavitation, acoustic measurements were conducted at low PRF (0.1 Hz) in water degassed to ~ 1.8–2.7 ppm (~ 20–30% of saturation). The sensitive 100 μm glass fiber tip of the FOPH was positioned at the target point F of the lithotripter (the fiber tip is faintly visible in Figure 1). Figure 2 shows an average temporal profile of lithotripter SW recorded at PL1. The lithotripter pulse had peak positive pressure (P+) approximately 40 MPa and peak negative pressure (P-) ~ 4 MPa. Increase in power level progressively increased both P+ and P-, reaching P+≈52 MPa and P-≈6.5 MPa at PL6 (waveforms not shown).

In order to assess the extent to which acoustic reflections within the test tank might contribute to the cavitation field, a series of extended time pressure traces were recorded covering 1 ms beyond the passage of the lithotripter shock pulse. FOPH traces were collected at the target point of the lithotripter at PL1 and averaged over 150 SWs. The amplitude of the reflected waves did not exceed 0.8 MPa, that is, was smaller than 2% of 40 MPa peak positive pressure of lithotripter SWs (inset in Figure 2), suggesting that the contribution of the reflected waves was not a substantial one.

RESULTS

Cavitation was affected by PRF and by the power level of the lithotripter. At very slow PRF, such as shots fired many seconds apart, cavitation was relatively sparse and typically did not noticeably increased for subsequent shots. As has been observed in previous studies, cloud amplification occurred when PRF was increased,[1–5] but also when the power level was increased. Figure 3 shows bubble clouds produced at PL2 (top) and PL6 (bottom) by two consecutive SWs at 2 Hz PRF. The bubble clouds generated by one SW (left) were amplified by the subsequent SW (right), with PL6 (bottom) producing more bubbles than PL2 (top).

Shot-to-shot amplification of bubble cloud was due to daughter microbubbles that were produced upon collapse and rebound of cavitation bubbles.[5] These daughter microbubbles were seen to migrate across the field seeding the proliferation of cavitation upon being hit by successive shock waves (Figure 4).

The pattern of bubble migration depended on PRF and PL. At slow PRF, cavitation was relatively sparse and microbubbles flowed in the direction of SW propagation before they drifted upward and away from the SW-axis. An increase in cavitation was accompanied by an apparent change in the pattern of bubble migration. Whereas bubbles continued to enter the field of view from the prefocal side, the main bubble cloud remained near the focal point. That is, the main cloud did not migrate across the field. One can see bubbles starting to move in the direction opposite to the SW-propagation in the postfocal portion of the field. This streaming of bubbles opposite to the direction of SW propagation appears to block the migration of the main cloud, which grew somewhat under the influence of successive SWs.

Figure 5 shows images of microbubbles (left) and flow velocities (right) immediately prior to the arrival of the fifth SW (t=1.985 s) at 2 Hz PRF. Bubbles to the right of the main cloud flowed from right to left (in the direction of SW-propagation, blue arrows), while bubbles to the left of the cloud flowed in the opposite direction (red arrows).

After several SWs at 2Hz PRF, cavitation flows at PL2 created a cloud centered approximately 15 ± 3 mm prefocal, so that bubbles flowed from both directions on the SW-axis toward one dynamic region located ~ 15 mm prefocally (Figure 6, top panels). PL6 continued to grow the cavitation field and enhanced the flow of bubbles opposite to the direction of SW propagation (Figure 6, bottom panels). Indeed, bubble flow originating postfocally (left to right flow) appeared to build and then overcome the flow from the prefocal side (right to left flow). This acted to push the broad cloud that had formed by shot 5 (centered ~ 15 mm prefocal, Figure 5) progressively to the right at a rate of about 10 mm/s, such that by SW 10 the plane of the interface between prefocal and postfocal bubble flows was outside the right margin (prefocal side) of the field of view (Figure 6).

Figure 6 shows cavitation flows recorded immediately prior to the arrival of the 10th and 11th SWs at 2 Hz PRF. By this time, the induced flows somewhat stabilized so that the magnitudes and directions of the induced flows remained approximately the same from SW to SW. The maximum flow velocity was measured at PL6 in the direction opposite to the SW-propagation and was about 30 mm/s (relative magnitude is shown by the length of the arrows).

The position of the plane at which the opposing directional bubble flows collided was dependent on the power level of the lithotripter. Figure 7 shows images of cavitation clouds recorded prior to the arrival of the ~ 15th SW at 2 Hz PRF at all six power levels of the lithotripter (PL1–PL6). At this PRF, the opposing cavitation flows collided prefocally at all power levels. Stepping up the PL acted to push the broad cloud progressively prefocally (to the right, Figure 7), shifting the position of the plane at which the opposing directional bubble flows collided toward the SW-source. Thus, increasing the power level acted to move the main bubble cloud closer to the SW-source.

DISCUSSION

It is observed that cavitation clouds generated by lithotripter SWs can induce streaming. Figures 3–6 show snapshots of the induced streaming at 2 Hz PRF at two power levels of the lithotripter: PL2 and PL6. The formation of the streaming at PL1 can be seen in the movie Mm. 3 of Reference 5. That movie shows 25 consecutive SWs at 2 Hz PRF capturing a transformation of a single bubble into a dense cavitation cloud. During these 25 shots the center of the bubble cloud continued to move along the direction of SW-propagation (from right to left). However, as the number of bubbles increased from shot-to-shot, bubbles located to the left of the cloud center started to flow in the direction opposite to SW-propagation (from left to right). This "reversed" streaming—directed opposite to the SW-propagation—began to stabilize the position of the main bubble cloud at the prefocal region of the lithotripter.

We speculate that potential mechanisms responsible for the observed streaming can be divided into two groups. The first group includes effects associated with the direct interaction of SWs with cavitation clouds. Such mechanisms will be discussed elsewhere. The second group includes some potential mechanisms related to the dynamics of bubble clouds in SWL. One such observation is that cloud collapse starts at the periphery of the cloud and proceeds to the cloud center.[2] The collapsing bubbles were seen to jet and move toward the neighboring bubbles, dragging the surrounding liquid toward the next—yet to collapse—layer of bubbles. This dynamic of bubble clouds in SWL has been observed using high-speed imaging.[1–7] To help appreciate this dynamic, the reader is encouraged to download movie Mm. 1 of Reference 2 showing the growth and collapse of a cavitation cloud. Comparing frames 120 μs and 250 μs, one can see that larger bubbles (mostly located along the SW axis) continue to grow while smaller bubbles (mainly located at the periphery of the cloud) have started to collapse. In subsequent frames the cloud collapse proceeds layer-by-layer toward the centrally located cavities on the SW-axis (frames 380 μs, 510 μs, and 640 μs). Finally, at 770 μs after the passage of the lithotripter SW, only the last remaining cluster of bubbles is visible ~ 8 mm prefocal. We refer to this position of the last visible bubbles as the cloud center. In the last four frames (380–770 μs), the bubble cloud was ellipsoidal in shape, elongated along the SW-axis. The collapse of this "cigar-shaped" cloud proceeded toward the cloud center located prefocally (at the bottom of the frames), forming a flow along the SW-axis in the direction opposite to SW-propagation. The direction of flow can be tracked, to some degree, by the motion of bubbles between the consecutive frames, in which some collapsed bubbles were seen to move on the order of 1 mm. This is not surprising considering the space occupied by bubbles, and that when bubbles collapse the fluid in the surround should rush in to fill the void.

As the bubbles grow, collapse, and rebound they are attracted to each other by Bjerknes forces. This would act to move the bubbles to the center of the cloud. In addition to this motion, the collapsing bubbles were observed to jet. Figures 2 and 3 of Reference 7 show the direction and timing of bubble jetting in cavitation clouds: the bubbles jet toward the "gravity" center of the cloud, with smaller bubbles collapsing first. When a smaller bubble collapsed in the vicinity of a larger bubble, a microjet from the smaller bubble was seen to break the spherical symmetry of the larger bubble long before its first inertial collapse (Figure 3 in Reference 7). In bubble clouds, as the collapse proceeded from the periphery to the center of the cloud, the collapsing bubbles were seen to emit jets toward the neighboring —yet to collapse—bubbles. This and other images suggest that bubble jetting may noticeably contribute to the formation of the observed flows.

Indeed, jetting bubbles were seen to move in the direction of the jet as far as ~ 1mm within only a few tens or hundreds of μs. Such bubble motion—along the direction of their jets— can be seen in high-speed camera sequences shown in References 5 and 6. The left panel of movie Mm. 1 (Reference 5) shows the collapse of a 1-mm bubble creating a jet upon rebound (frame 248 μs) and a cloud of daughter microbubbles (frame 788 μs) with the cloud center displaced in the direction of the jet at ~ 1 mm from the original position of the parent bubble. A jet during the collapse of a smaller (~ 0.25 mm) bubble—shown on the right panel of the movie—produced fluid motion that moved the generated cloud of daughter microbubbles at ~ 0.5 mm from the original position of the parent bubble. Thus, high-speed

camera images show that jets create flows in the vicinity of the collapsing bubbles with velocities on the order of m/s, which is two orders of magnitude higher than the flow velocities (~ 30 mm/s) observed here at about half a second after the collapse of the bubbles (Figures 5–6).

Cavitation flows of the same order of magnitude have been measured using particle image velocimetry (PIV) after a passage of a single lithotripter pulse. Buick et al[9] observed a uni-directional flow 40 ms after the passage of the pulse flowing in the direction of SW propagation with maximum velocity of 25 mm/s. Velocities of 100 mm/s were measured in localized flows associated with growth and collapse of cavitation bubbles at time intervals on the order of milliseconds after the passage of the pulse.[9] Arora et al[10] also observed maximum velocities near the cores of cavitation-induced vortices, although they found that the maximum velocities increased from ~ 30 mm/s to 50 mm/s during the first 0.2 s after the passage of the lithotripter pulse (Figure 10 in Reference 10). At 0.5 s after the passage of the pulse, maximum flow velocities were in the range of 20–30 mm/s.[10]

Arora et al[10] observed that a passage of a single lithotripter pulse generated flow patterns with counter-rotating vortices. Buick et al[9] reported that these localized flows evolve into a uni-directional flow in the direction of propagation of lithotripter pulse. We observed that the pattern of the induced flows depended on PRF and power level of the lithotripter. Low PRF and low PL generated sparse cavitation clouds that generally migrated in the direction of SW-propagation. Higher PRF and PLs generated denser cavitation clouds that—in addition to the flow along the SW-axis—also induced "reversed streaming" in the direction opposite to the propagation of lithotripter SWs.

A flow pattern with counter-rotating vortices prompted Arora et al[10] to speculate that the mixing flows would introduce fresh cavitation nuclei into the focal area of the lithotripter. We visualized the motion of cavitation nuclei—daughter microbubbles—at different PRFs and power levels of the lithotripter. At low PRFs and low PLs cavitation nuclei drifted through the focal area of the lithotripter in the direction of SW-propagation. That is, microbubbles from previous SWs were washed away from the focal region of the lithotripter while new clouds of microbubbles were brought from the prefocal region of the lithotripter.

At fast PRF (2 Hz) cavitation nuclei were carried through the focus F of the lithotripter in the direction opposite to the SW-propagation. At this PRF cavitation nuclei were flowing from both sides of the SW-axis into one dynamic region located prefocally. The position of this region shifted toward the SW-source with increase in PL.

In summary, it is observed that cavitation clouds generated by lithotripter SWs can induce streaming and the induced streaming can be directed opposite to SW-propagation. With the caveat that these measurements were conducted in non-degassed water under free-field conditions, the present study suggests that cavitation at SW-rates used in clinical SWL (0.5–2 Hz PRF) can be accompanied by substantial flows, the pattern of which depends on PRF and power level of the lithotripter. This suggests that not only does increased PRF and higher PL create more bubbles, these new bubbles are not randomly dispersed, but tend to

aggregate—and this could potentially create a more robust barrier for delivering SW energy to kidney stones.

ACKNOWLEDGMENTS

REFERENCES

1. Sapozhnikov OA, Khokhlova VA, Bailey MR, Williams JC Jr., McAteer JA, Cleveland RO, and Crum LA, "Effect of overpressure and pulse repetition frequency on cavitation in shock wave lithotripsy," J. Acoust. Soc. Am 112 (3), 1183–1195 (2002). [PubMed: 12243163]

2. Pishchalnikov YA, Sapozhnikov OA, Bailey MR, Pishchalnikova IV, Williams JC Jr., and McAteer JA, "Cavitation selectively reduces the negative-pressure phase of lithotripter shock pulses," Acoustic Research Letters Online 6, 280–286 (2005).

3. Pishchalnikov YA, McAteer JA, Williams JC Jr., Pishchalnikova IV, and VonDerHaar RJ, "Why stones break better at slow shock wave rate than at fast rate: In vitro study with a research electrohydraulic lithotripter," J. Endour 20, 1–5 (2006).

4. Pishchalnikov YA, McAteer JA, and Williams JC Jr., "Effect of firing rate on the performance of shock wave lithotriptors," BJU Int. 102 (11), 1681–1686 (2008). [PubMed: 18710450]

5. Pishchalnikov YA, Williams JC Jr., and McAteer JA, "Bubble proliferation in the cavitation field of a shock wave lithotripter," JASA-EL 130 (2), EL1–7 (2011).

6. Pishchalnikov YA, Neucks JS, VonDerHaar RJ, Pishchalnikova IV, Williams JC Jr., and McAteer JA, "Air pockets trapped during routine coupling in dry-head lithotripsy can significantly reduce the delivery of shock wave energy," J. Urol 176, 2706–2710 (2006). [PubMed: 17085200]

7. Gui LC, Merzkirch W, "A method of tracking ensembles of particle images," Experiments in fluids 21, 465–468 (1996).

8. Pishchalnikov YA, Sapozhnikov OA, Bailey MR, McAteer JA, Williams JC Jr., Evan AP, Cleveland RO, and Crum LA, "Interactions of cavitation bubbles observed by high-speed imaging in shock wave lithotripsy," In: Innovations in Nonlinear Acoustics (Proceedings of 17th International Symposium on Nonlinear Acoustics, State College, Pennsylvania, 18–22 July 2005), Amer. Inst. of Physics conference proceedings 838, pp.299–302 (2006). 10.1063/1.2210365

9. Buick J, Cosgrove J, Eizenhöfer H, Higham R and Royles R, "Characterization of the bubble cluster and velocity field in the focal region of a lithotripter," New Journal of Physics 9, 240 (2007).

10. Arora M, Junge L and Ohl CD, "Cavitation cluster dynamics in shock-wave lithotripsy: part 1. Free field," Ultrasound Med Biol 31, 827–839 (2005). [PubMed: 15936498]
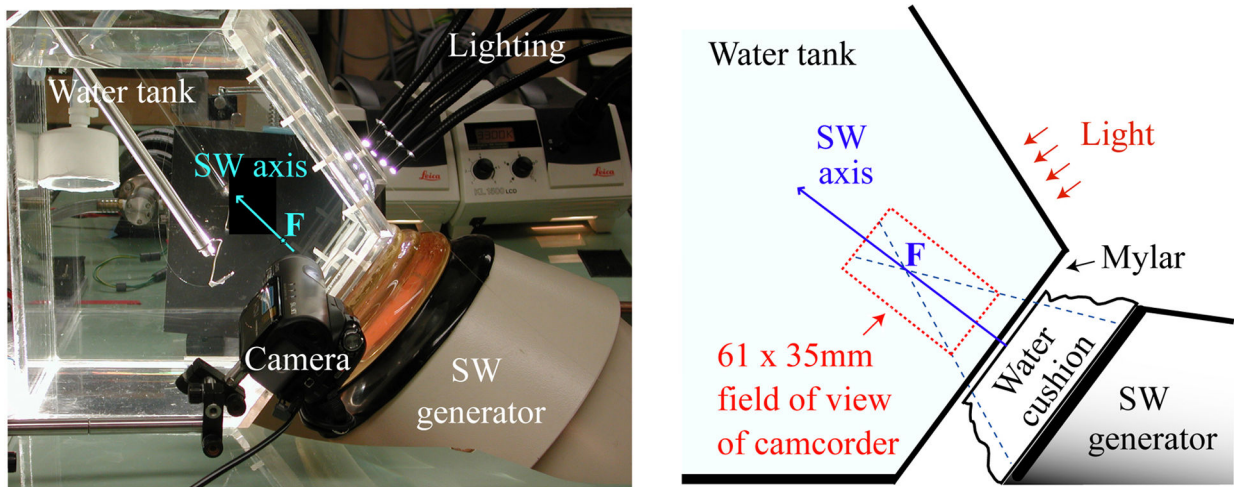
FIGURE 1.
Photo (left) and a sketch (right) of the experimental setup. The water cushion of the SW generator (therapy head) was coupled to the Mylar acoustic window of the test tank using LithoClear gel. As the acoustic axis of the lithotripter (SW-axis) was at 45° from vertical, the camcorder was tilted so that SW would be seen to propagate from right to left. The field of view of the camcorder was 61 × 35 mm. F marks the target point of the lithotripter. Lighting was provided by two twin fiber-optic light sources (KL 1500 LCD, Leica) positioned above the target zone of the lithotripter and oriented approximately perpendicular to the SW axis.
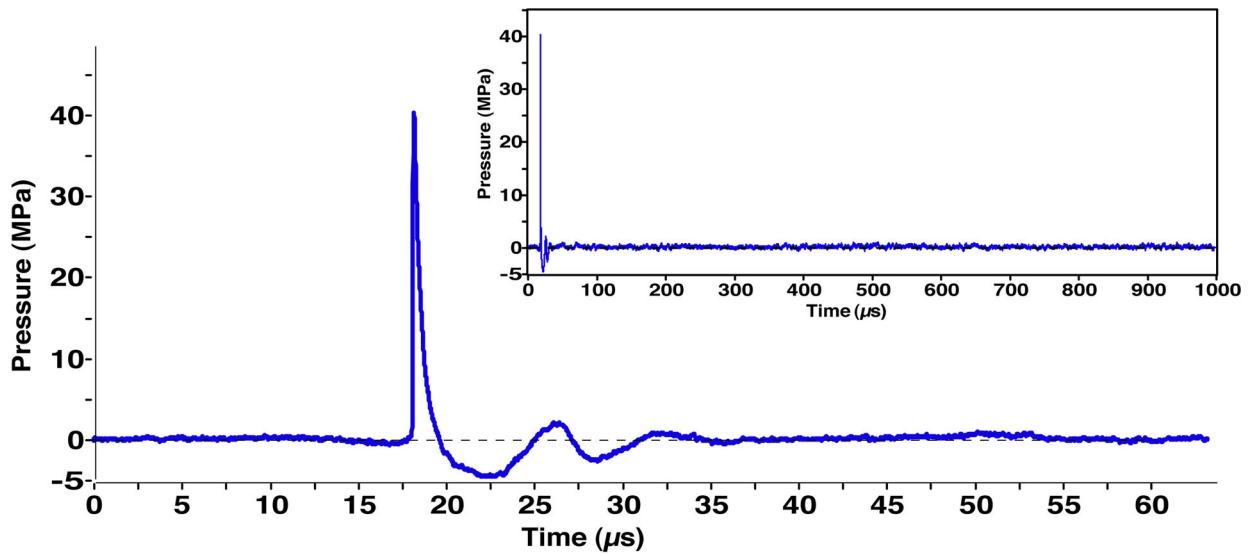
FIGURE 2.
Averaged temporal profile (150 SWs, 0.1Hz PRF) recorded at PL1 at the target point F of the lithotripter. The inset shows the same FOPH trace covering ~1 ms beyond the passage of the lithotripter shock pulse. The amplitude of the reflected waves did not exceed 0.8 MPa, that is, was smaller than 2% of ~ 40 MPa peak positive pressure of lithotripter SWs, suggesting that the contribution of the reflected waves was not a substantial one.
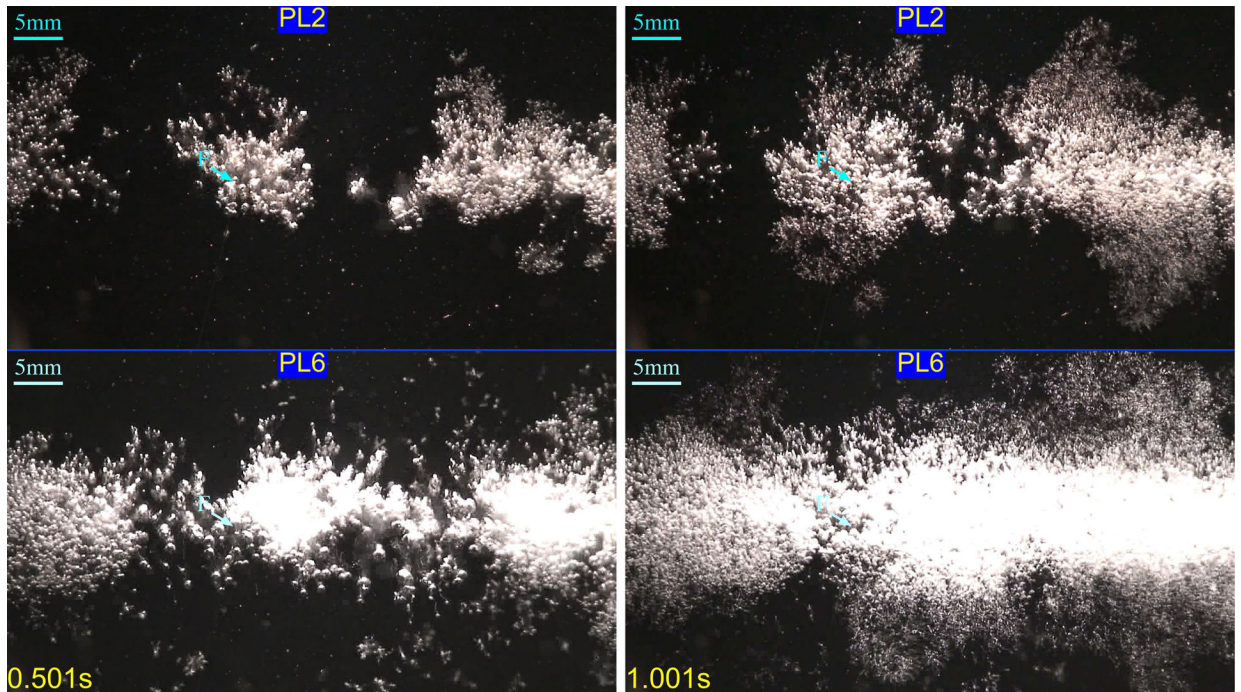
FIGURE 3.
Bubble clouds produced at PL2 (top) and PL6 (bottom) by the second (t=0.5 s, left) and the third (t=1 s, right) SWs at 2 Hz PRF. The bubble clouds generated by one SW (left) were amplified by the subsequent SW (right). PL6 (bottom) produced more bubbles than PL2 (top), showing that stepping up the PL grew the cavitation field and enhanced the cloud amplification.
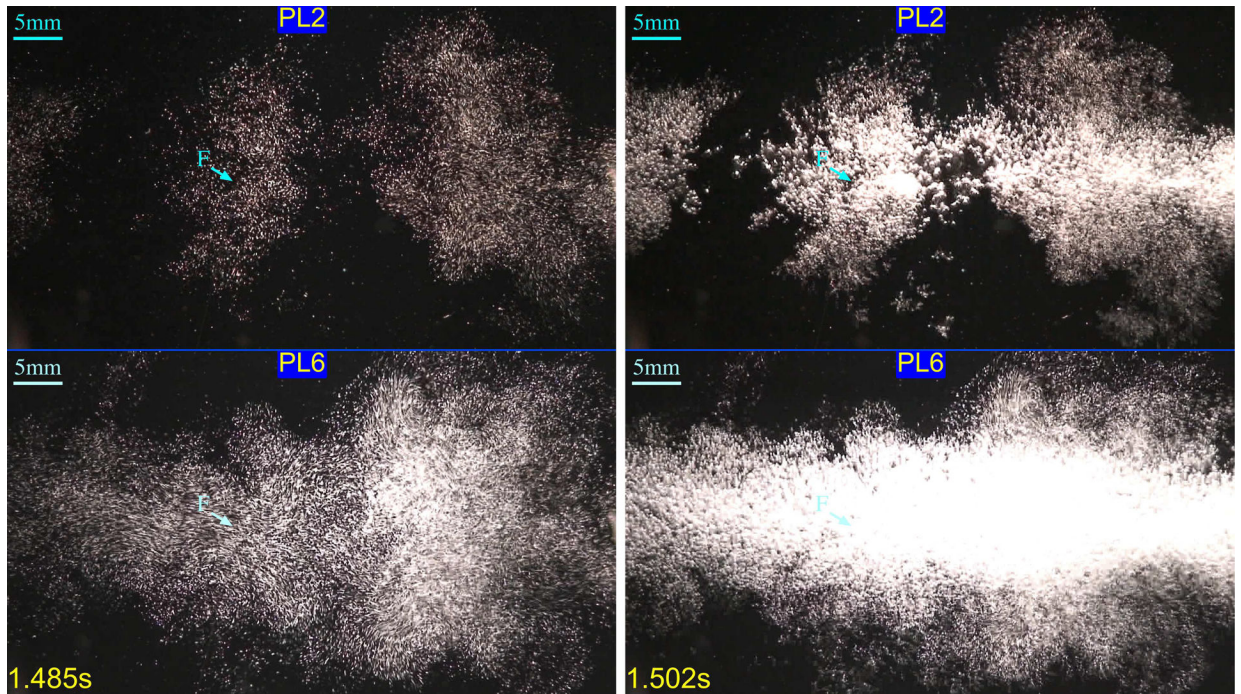
FIGURE 4.
Bubble clouds at PL2 (top) and PL6 (bottom) immediately prior to (t=1.485 s, left) and during (t=1.502 s, right) the passage of the fourth SW at 2 Hz PRF. Microbubbles (left panel) gave rise to the cavitation bubbles seen on the right panel.
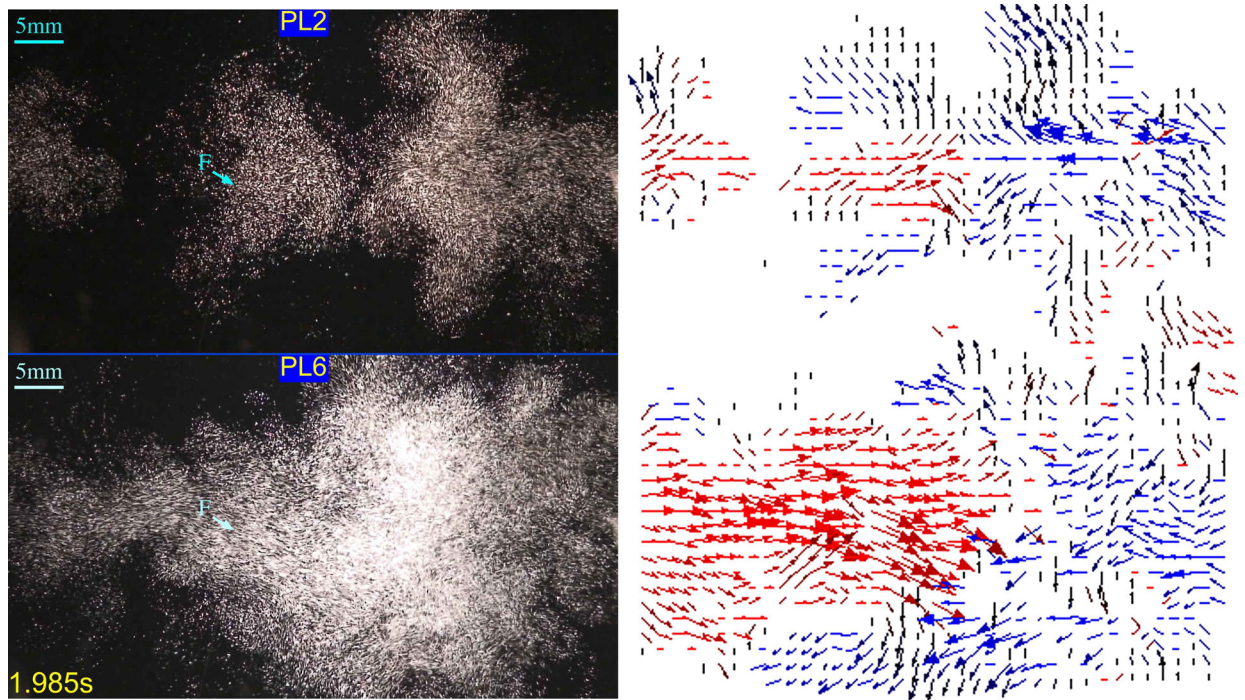
FIGURE 5.
Clouds of microbubbles at PL2 (top) and PL6 (bottom) immediately prior to the arrival of the fifth SW at 2 Hz PRF. Right panel shows flow velocities: red arrows show flows opposite to the direction of SW-propagation, blue arrows show flows directed along the passage of the SW, and black arrows show lateral flows.
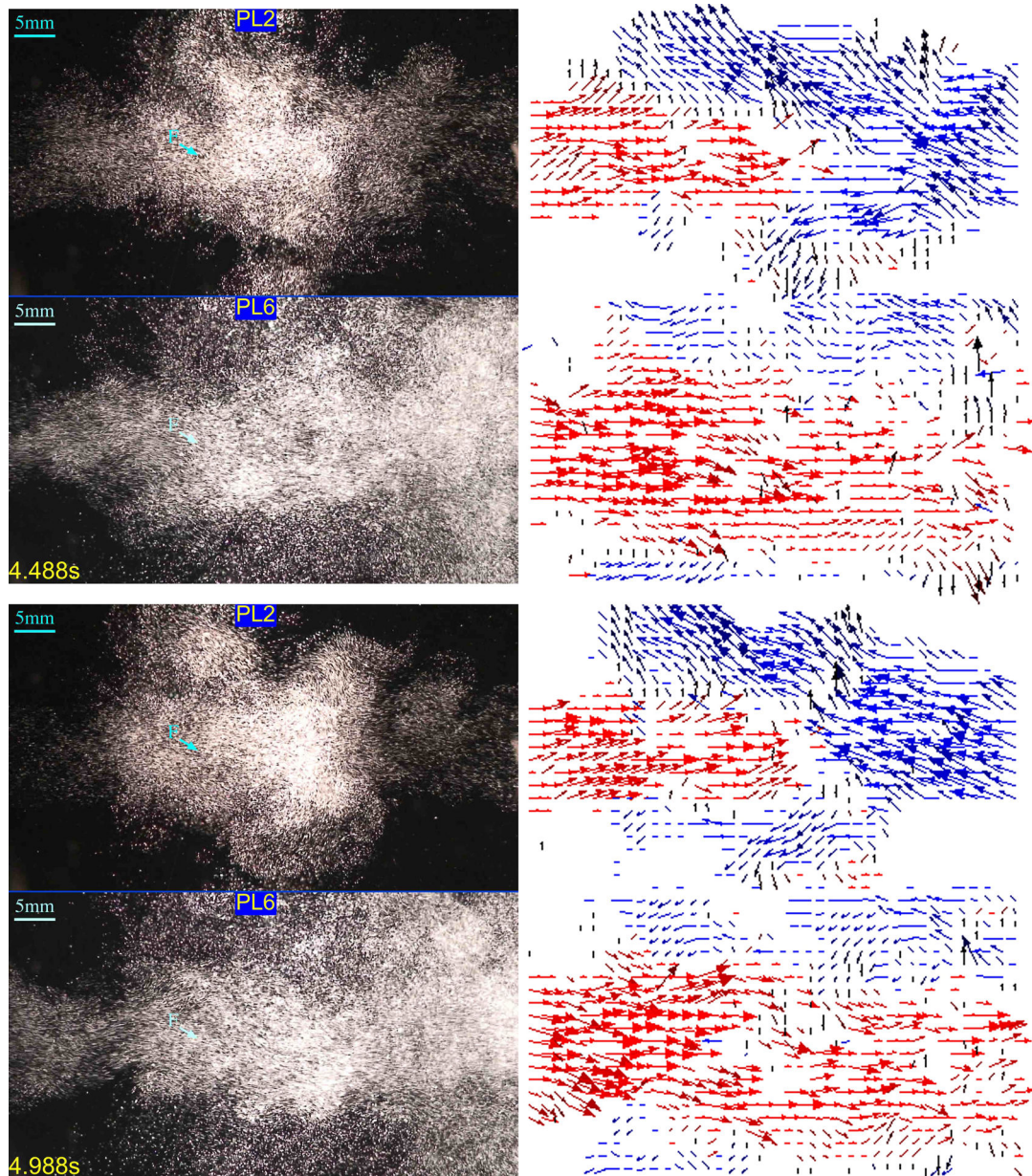
FIGURE 6.
Clouds of microbubbles at PL2 and PL6 immediately prior to the arrival of the 10th (t=4.488 s, top) and 11th (t=4.988 s, bottom) SWs at 2 Hz PRF. Right panel shows flow velocities: red arrows show flows opposite to the direction of SW-propagation, blue arrows show flows directed along the passage of the SW, and black arrows show lateral flows.
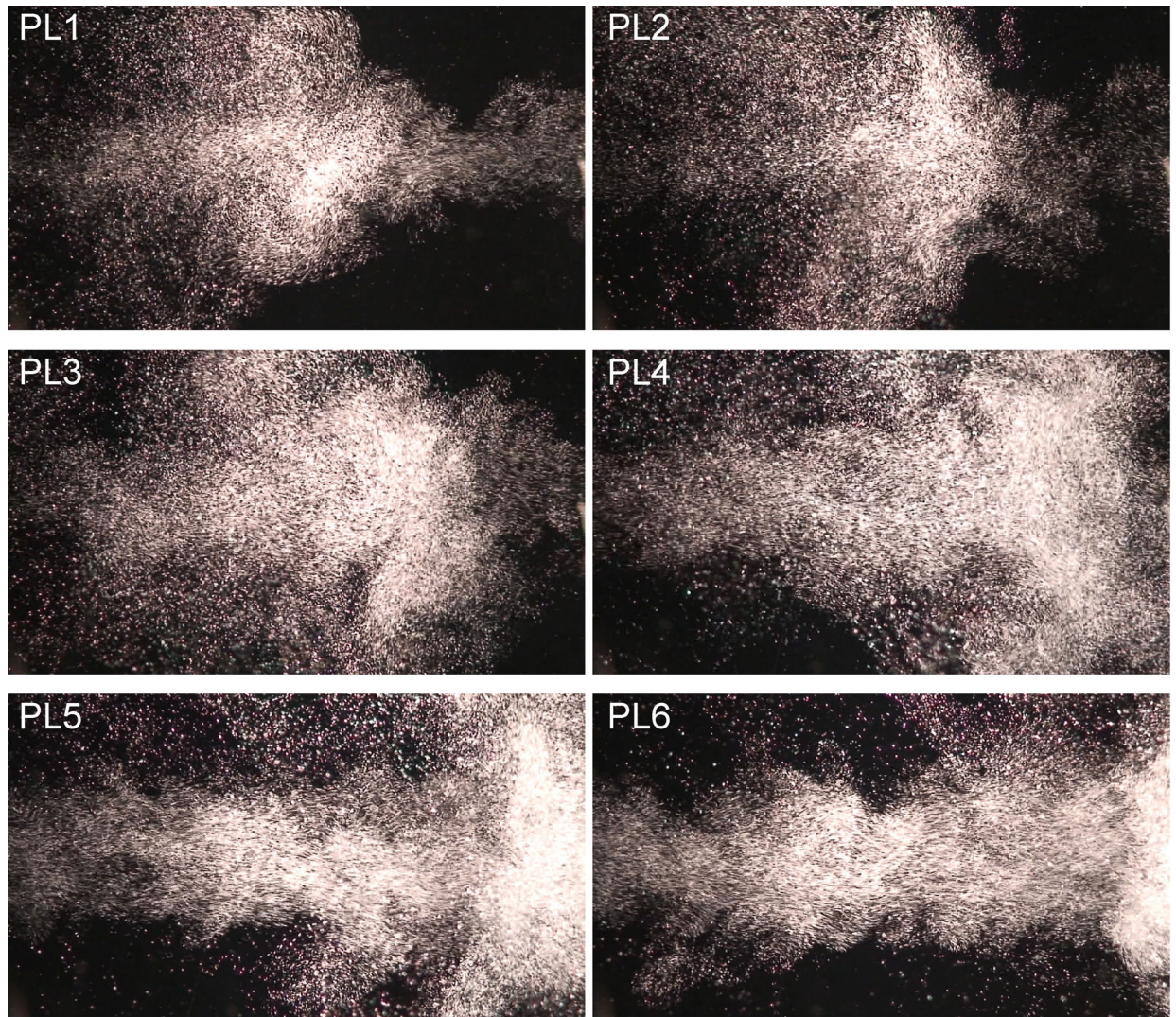
FIGURE 7.
Typical cavitation clouds recorded between lithotripter SWs at 2 Hz PRF at six power levels (PL1–PL6). Increasing the power level shifted the position of the center of the cloud toward the SW-source (to the right, shock waves propagated from right to left in these images). This was due to a streaming of bubbles opposite to the direction of SW propagation. Stepping up the PL grew the cavitation field and enhanced the flow of bubbles opposite to the direction of SW propagation. This acted to push the position of the plane at which the opposing directional bubble flows collided closer to the SW-source, shifting the broad cloud progressively prefocally (toward the SW source).